

ARTICLE

Received 19 May 2016 | Accepted 28 Nov 2016 | Published 19 Jan 2017

DOI: 10.1038/ncomms14089

OPEN

Direct PIP₂ binding mediates stable oligomer formation of the serotonin transporter

Andreas Anderluh¹, Tina Hofmaier², Enrico Klotzsch³, Oliver Kudlacek², Thomas Stockner², Harald H. Sitte^{2,*} & Gerhard J. Schütz^{1,*}

The human serotonin transporter (hSERT) mediates uptake of serotonin from the synaptic cleft and thereby terminates serotonergic signalling. We have previously found by single-molecule microscopy that SERT forms stable higher-order oligomers of differing stoichiometry at the plasma membrane of living cells. Here, we report that SERT oligomer assembly at the endoplasmic reticulum (ER) membrane follows a dynamic equilibration process, characterized by rapid exchange of subunits between different oligomers, and by a concentration dependence of the degree of oligomerization. After trafficking to the plasma membrane, however, the SERT stoichiometry is fixed. Stabilization of the oligomeric SERT complexes is mediated by the direct binding to phosphoinositide phosphatidylinositol-4,5-bisphosphate (PIP₂). The observed spatial decoupling of oligomer formation from the site of oligomer operation provides cells with the ability to define protein quaternary structures independent of protein density at the cell surface.

¹Institute of Applied Physics, TU Wien, Wiedner Hauptstrasse 8-10, Vienna 1040, Austria. ²Center for Physiology and Pharmacology, Institute of Pharmacology, Medical University Vienna, Waehringerstrasse 13A, Vienna 1090, Austria. ³EMBL Australia Node in Single Molecule Science, School of Medical Sciences, ARC Centre of Excellence in Advanced Molecular Imaging, University of New South Wales, Sydney, New South Wales 2052, Australia. * These authors contributed equally to this work. Correspondence and requests for materials should be addressed to H.H.S. (email: harald.sitte@meduniwien.ac.at) or to G.J.S. (email: schuetz@iap.tuwien.ac.at).

The human serotonin transporter (SERT) is a 12-pass transmembrane protein targeted to presynaptic nerve terminals and belongs to the neurotransmitter: sodium symporter (NSS) or solute carrier 6 (SLC6) family¹. These transmembrane proteins mediate the high-affinity uptake of neurotransmitters from the synaptic cleft and are, hence, of pivotal importance for synaptic signal transmission by terminating chemical signal transduction between neurons. SERT is the target for antidepressants like serotonin-selective reuptake inhibitors² as well as for illicitly used drugs such as amphetamines³; the latter act by reversing the transport direction of SERT, provoking release of serotonin (5-HT) into the extracellular space⁴.

Biochemical and spectroscopic studies have reported that SERT is present as oligomeric complexes at the plasma membrane^{5–9}. Likewise, oligomerization of a number of other NSS family members has been described¹⁰. The oligomeric state, however, does not seem to be crucial for uptake activity: for example, it was found that oligomerization-deficient mutants of the GABA transporter (GAT1) retain unchanged transport activity¹¹. Currently, two possible roles of NSS oligomerization are discussed: (i) oligomerization of correctly folded proteins is necessary to pass the quality control for trafficking from the endoplasmic reticulum (ER)¹², in the case of SERT specifically by allowing the interaction with SEC24C (refs 13,14). (ii) It has been reported that oligomerization is a prerequisite for the reverse operation of the transporter which affords substrate release¹⁵.

Using single-molecule fluorescence microscopy, we have previously discovered that SERT forms a broad distribution of assemblies ranging from monomers up to pentamers⁷. The homo-association at the plasma membrane did not depend on SERT surface density and was stable at least over 10 min. We proposed a model based on kinetic trapping of oligomers at the plasma membrane, subsequent to an equilibration which occurred at an unknown subcellular organelle. The site of equilibration and the mechanism behind kinetic trapping, however, remained unclear.

Some arguments pointed our interest to the negatively charged phospholipid phosphatidylinositol-4,5-bisphosphate (PIP₂). PIP₂ is part of a number of signalling pathways, for example, endo- and exocytosis, cell adhesion, cell motility, phagocytosis or G protein-coupled receptor signalling¹⁶. It is a minor phospholipid that is mainly found at the cytoplasmic leaflet of the plasma membrane, where it occurs at a surface density of about $\sigma_{PIP_2} \sim 20,000\text{--}60,000$ molecules μm^{-2} (ref. 17). Pronounced differences exist in the subcellular localization of PIP₂: PIP₂ comprises about 1% of total lipid at the plasma membrane¹⁷, whereas only trace amounts of PIP₂ are present at the ER¹⁸. PIP₂ binding to transmembrane proteins is frequently observed, for example, for ion channels, where it regulates channel activity by influencing the open probability¹⁹. Likewise, we have recently found that the functional activity of SERT and the dopamine transporter (DAT) was influenced by PIP₂ binding^{20,21}: upon enzymatic depletion of PIP₂ or mutation of identified PIP₂ binding sites, amphetamine-induced substrate efflux was markedly reduced whereas uptake rates were essentially unaffected. Similarly, while the oligomeric configuration does not seem to influence neurotransmitter uptake¹¹, amphetamine-induced neurotransmitter release has been shown to rely on the quaternary arrangement¹⁵.

In the present study, we quantify the degree of SERT oligomerization at different subcellular localizations of Chinese hamster ovary (CHO) cells and analyse the kinetics of protomer turnover. We find evidence that SERT oligomers are pre-formed at the ER following a dynamic equilibrium model. At the plasma membrane, kinetic trapping arrests the oligomers at the

pre-set stoichiometry. Our data suggest that the different subcellular concentrations of PIP₂ mediate the differential SERT oligomerization behaviour, likely by direct physical connection of SERT protomers.

Results

SERT oligomerization depends on subcellular localization.

First, we addressed if SERT oligomerization differs between the plasma membrane and the ER. Monomeric GFP (mGFP) was inserted at the cytosolic N-terminus of SERT to allow for visualization (mGFP–SERT)²². Plasma membrane-localized mGFP–SERT was recorded at the bottom cell membrane via total internal reflection fluorescence (TIRF) microscopy. To retain SERT in the ER, we overexpressed a dominant-negative mutant of Sar1a (Sar1a-T39N)¹³, a small GTPase that regulates the assembly of COPII vesicles for plasma membrane trafficking. Sar1a-T39N is a GDP-restricted mutant which prevents the formation of COPII in a dominant-negative manner, thereby arresting SERT in the ER. ER-retained mGFP–SERT was studied at junctions between ER and the plasma membrane, where single-molecule tracking at high signal-to-noise ratio using TIRF microscopy is feasible^{23,24}.

We used the ‘Thinning out clusters while conserving stoichiometry’ (TOCCSL) technique previously established in our lab^{7,25–27} to determine the oligomeric state of mGFP–SERT. TOCCSL extends fluorescence recovery after photobleaching (FRAP) to the level of single-molecule fluorescence microscopy (Fig. 1a). Typically, the high density of fluorescently labelled proteins results in a homogeneously labelled surface, thereby precluding direct single-molecule measurements (Fig. 1a,i). In TOCCSL, a small area of the cell membrane is irreversibly photobleached by a strong laser pulse focused through a rectangular pinhole onto the sample (Fig. 1a,ii,iii). The high laser intensity completely abrogates the fluorescence signal of the mGFPs in every SERT molecule within the illuminated area, while retaining full brightness outside this area. During the subsequent recovery phase unbleached molecules and oligomers diffuse into the previously bleached area due to Brownian motion (Fig. 1a,iv). In contrast to FRAP experiments, however, we exploit in TOCCSL the very onset of this recovery process, when individual molecules can be monitored as single, clearly distinguishable fluorescent spots (Fig. 1a,v). The brightness of these spots was determined and compared with the brightness of single mGFP–SERT molecules recorded under the same conditions and in the same subcellular compartments, yielding the statistical distribution of mGFP–SERT oligomers. Note that, similar to fluorescence correlation experiments, TOCCSL allows only analysis of the mobile fraction of molecules.

We used this experimental strategy to determine the mean aggregation size of mGFP–SERT located at the plasma membrane (Fig. 1b, left) or retained at the ER (Fig. 1b, right) of CHO cells. The differences in the subcellular distributions are apparent in TIRF microscopy; while plasma membrane-localized SERT yields a homogenous intensity distribution over the whole interface of the cell with the glass slide (Fig. 1b, left), we observed the characteristic reticular ER–plasma membrane junctions upon Sar1a-T39N overexpression (Fig. 1b, right). The majority of the protein was freely mobile in both cellular compartments, yielding mobile fractions of $82 \pm 8\%$ and $66 \pm 12\%$ (s.e.m.; $n \geq 10$ cells) for plasma membrane and for the ER in FRAP experiments, respectively.

We first confirmed our recent finding of SERT oligomerization at the plasma membrane: the left panel of Fig. 1b shows the brightness distribution, plotted as a probability density

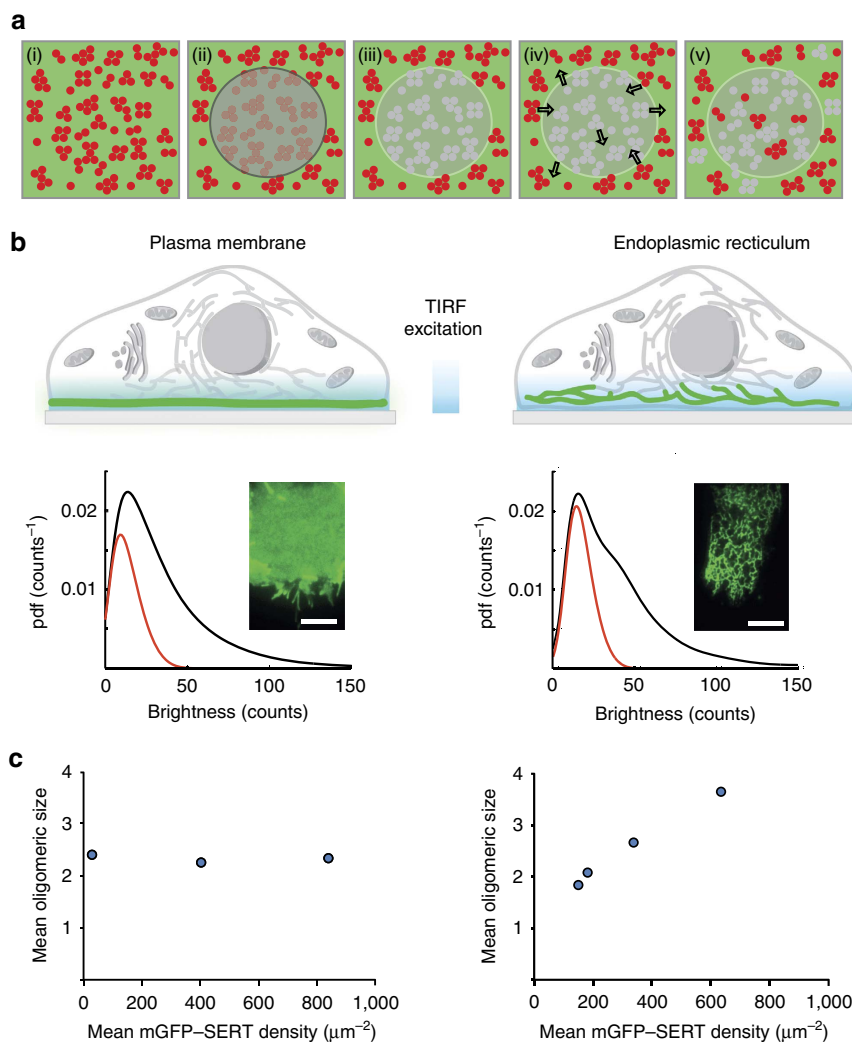


Figure 1 | Determination of mGFP-SERT oligomer sizes by single molecule brightness analysis. (a) Thinning out clusters while conserving stoichiometry of labeling (TOCCSL). Using a field stop in the laser beam pathway, a small area of the densely fluorescently labelled cell membrane (i) is irreversibly photobleached (ii, iii). During the recovery phase (iv), SERT oligomers diffuse back into the bleached area. At the onset of this process, they can be discriminated as single, well separated fluorescent spots (v). (b) The oligomeric state of SERT was evaluated in the plasma membrane (left panel) or the endoplasmic reticulum (right panel) by single-molecule brightness analysis. The brightness distributions (in counts) of mGFP-SERT complexes are plotted as pdf. The plots show the distribution of the complexes from the TOCCSL image after the recovery phase (black curves) and the measured brightness of a monomer (red curves); see also Supplementary Fig. 3. A fit yields the distribution of oligomeric sizes at the respective organelle. Scale bars, 10 μm .

(c) At the plasma membrane, the mean oligomeric size is independent from the density of SERT ($n > 22$ cells per datapoint; plotted protein densities were 29 ± 17 (s.e.m.) μm^{-2} , $402 \pm 31 \mu\text{m}^{-2}$ and $840 \pm 56 \mu\text{m}^{-2}$; s.e.m. of the mean oligomeric sizes were smaller than 0.05). In contrast, at the ER higher expression levels correlate with larger oligomeric sizes ($n > 19$ cells per datapoint; plotted protein densities are 153 ± 13 (s.e.m.) μm^{-2} , $185 \pm 24 \mu\text{m}^{-2}$, $343 \pm 37 \mu\text{m}^{-2}$ and $643 \pm 36 \mu\text{m}^{-2}$; s.e.m. of the mean oligomeric sizes were smaller than 0.05).

function (pdf) obtained from the TOCCSL images. A large spread in the oligomer distribution was observed, and the mean oligomeric size did not depend on SERT surface density (Fig. 1c, left). The results were strikingly different, when we determined SERT oligomerization at the ER membrane. While the overall oligomer distribution remained highly heterogeneous (Fig. 1b, right), we found a pronounced increase of SERT oligomer size with increasing mean SERT density at the ER (Fig. 1c, right).

A second hallmark of dynamic size equilibration would be the exchange of subunits. To discriminate between stable association and rapid subunit exchange, we used the previously established method of repetitive TOCCSL runs⁷ (Fig. 2a). We performed one run per minute (each consisting of a single bleaching pulse and a single recovery image) over 10 min on the

very same cell. Pooling data from multiple cells provided brightness distributions as a function of time. By this procedure, the amount of active fluorophores per cell was substantially reduced to about 50%. In this approach, stable interaction of subunits would reduce the total number of observed spots, but would not alter the brightness distribution (Fig. 2a, scenario i). If the exchange rate of subunits was high, however, bleached subunits would mix with unbleached subunits. Over time, this mixing would increase the number of complexes containing both dark and fluorescent subunits, thereby shifting the observable oligomeric distribution towards smaller structures (Fig. 2a, scenario ii). At the plasma membrane, we observed no change in the oligomeric state with increasing number of TOCCSL runs. We thereby confirmed our previous results which indicated stability of SERT oligomers at the minutes

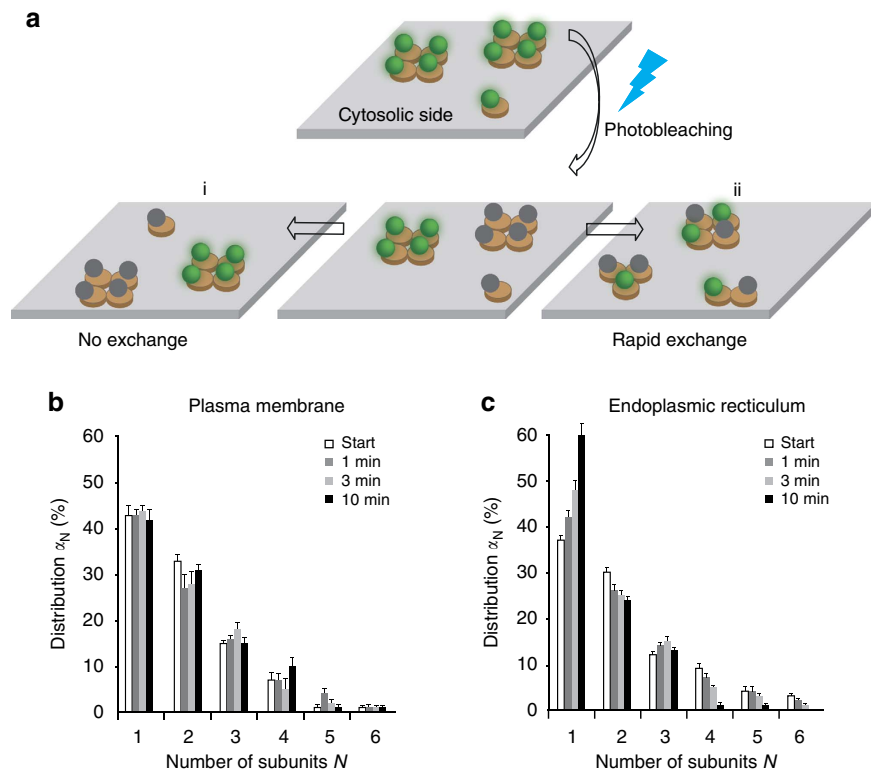


Figure 2 | Evaluation of the oligomer stability in the plasma membrane and at the ER. (a) To study the stability of SERT oligomers we performed repeated TOCCSL runs on the same cells (1 run per minute over 10 min), and determined the brightness distributions in each run. Two different scenarios can be distinguished: if oligomers were stable over the time course of the experiment, the total number of diffraction-limited spots would be reduced without altering the brightness distribution (left, scenario i). In contrast, if oligomers would exchange subunits during the 10 min, increasing numbers of mixed SERT oligomers containing both bleached and non-bleached subunits would be observable, thereby shifting the determined oligomeric distribution towards smaller structures (right, scenario ii). (b) Using the repetitive TOCCSL strategy, we have observed no change in the oligomeric distribution of SERT at the plasma membrane ($n = 20$ cells). Oligomeric distributions are shown at the beginning of the experiment (white bars), after 1 min (dark grey), 3 min (light grey), and after 10 min (black). (c) At the ER, however, we observed rearrangement of subunits over the timescale of the experiment, as can be seen by the shift of the distributions towards lower oligomer sizes ($n = 22$ cells). Error bars show the s.e.m.

timescale (Fig. 2b). At the ER membrane, however, we found a substantial shift towards oligomers with smaller amounts of active fluorophores, indicating rapid exchange of subunits between SERT oligomers (Fig. 2c).

Availability of PIP_2 affects SERT oligomerization. Given the described SERT- PIP_2 interaction²⁰ and the strong difference of PIP_2 levels between plasma membrane¹⁷ and ER¹⁸, we hypothesized that PIP_2 impacts on SERT oligomerization. We measured SERT oligomerization at the plasma membrane after depleting PIP_2 levels via activation of phospholipase $\text{C}\gamma$ (PLC γ) using the direct PLC γ -activator *m*-3M3FBS (ref. 28). PIP_2 depletion had no influence on the mean mGFP-SERT surface density (Supplementary Fig. 1). For low SERT surface densities (25 molecules μm^{-2}), we observed a marked shift of SERT oligomers towards smaller complexes, whereas application of the inert orthologue *o*-3M3FBS did not elicit any effect (38 molecules μm^{-2} , Fig. 3a). At higher SERT densities, however, oligomers increased in size (Fig. 3b), indicating rapid equilibration of the oligomerization reaction.

A consequence of rapid equilibration would be the continuous exchange of subunits between SERT oligomers. Hence, to test for the stability of oligomers we performed repetitive TOCCSL runs after incubating cells with *m*-3M3FBS. The quaternary arrangement of SERT in oligomers now showed rapid subunit

exchange (Fig. 3c), which indicated that SERT oligomers were indeed liberated from kinetic trapping. Together, these results show that PIP_2 depletion results in equilibration of SERT oligomerization and concomitant subunit exchange at the plasma membrane. Of note, SERT oligomerization at the plasma membrane lacking PIP_2 resembles the oligomerization behaviour at the ER membrane (Fig. 2).

PIP_2 binds directly to SERT and mediates oligomerization.

Next, we investigated whether direct PIP_2 binding to SERT sustained oligomer formation or whether PIP_2 would exert an indirect effect due to the downstream metabolites IP_3 or DAG. Recently, we identified the amino acids K352 and K460 as crucial residues for PIP_2 binding to SERT²⁰ (Fig. 4a); mutation of both residues to alanine yielded a substantial decrease of PIP_2 -induced effects on parachloroamphetamine-induced, SERT-mediated current and efflux. Most importantly, the PIP_2 -SERT interaction was shown to be greatly reduced in pull-down experiments²⁰. We used an mGFP-fusion construct of this mutant to evaluate the effect of reduced PIP_2 binding on the oligomeric state. The mGFP-tagged SERT-K352A-K460A double mutant was efficiently trafficked to the plasma membrane and showed similar uptake activity as the wild type²⁰. Single-molecule brightness analysis yielded an oligomeric distribution that differed from wild-type SERT (Fig. 4b): the dominant species

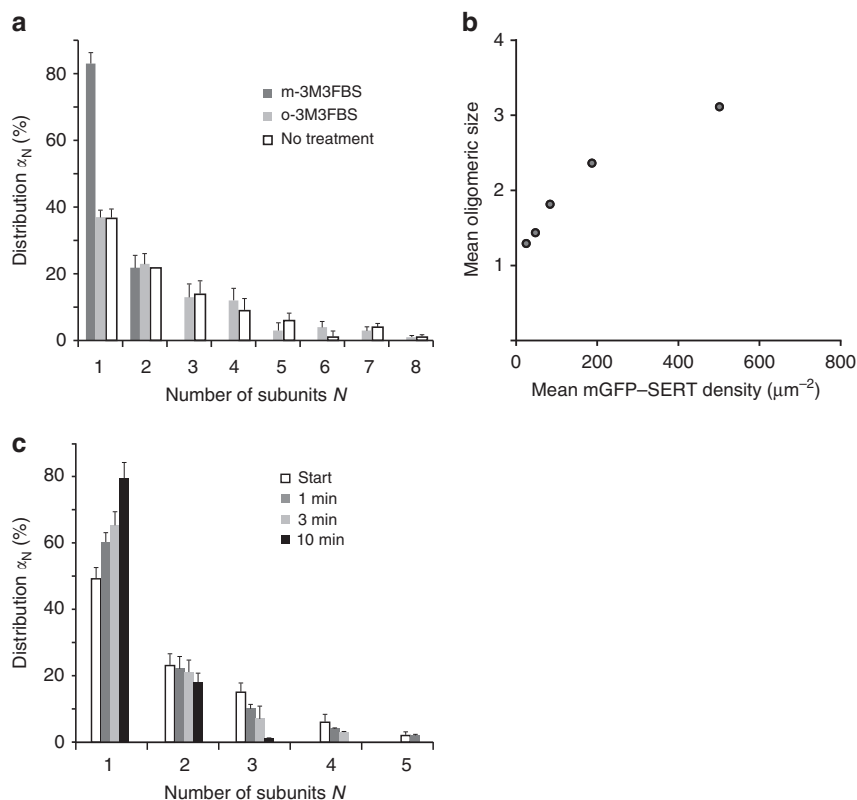


Figure 3 | SERT oligomerization at the plasma membrane depends on PIP₂ levels. (a) We enzymatically depleted PIP₂ at the plasma membrane via activation of phospholipase C_γ (PLC_γ) by incubating cells for 15 min with the direct PLC_γ-activator *m*-3M3FBS (10 μM). This led to a marked shift of SERT complex sizes towards monomers (dark grey bars). As a negative control, incubation with the inert orthologue *o*-3M3FBS did not yield any effect (light grey bars) in comparison to the untreated cells (white bars) ($n > 20$ cells per experimental condition). SERT surface densities were similar: 25 ± 14 (s.e.m.) μm⁻² (dark grey bars), 38 ± 22 μm⁻² (light grey bars), 29 ± 17 μm⁻² (white bars). (b) PIP₂ depletion via *m*-3M3FBS resulted in marked dependence of mGFP-SERT oligomerization on mGFP-SERT surface density ($n > 20$ cells per datapoint; plotted protein densities are 25 ± 14 (s.e.m.) μm⁻², 48 ± 24 μm⁻², 84 ± 17 μm⁻², 187 ± 28 μm⁻² and 501 ± 40 μm⁻²; s.e.m. of mean oligomeric sizes were smaller than 0.05). (c) To test for the effect of PIP₂ depletion on the stability of the oligomers at the plasma membrane, we performed repetitive TOCCSL runs upon incubating cells with *m*-3M3FBS (1 μM) ($n = 19$ cells). Now, the SERT complexes showed rapid subunit rearrangement, indicating liberation of SERT oligomers from kinetic trapping. The SERT surface density was 89 ± 21 (s.e.m.) molecules μm⁻². Error bars show the s.e.m.

are monomers and dimers, while the fraction of trimers and tetramers was reduced to almost baseline levels. The double mutant showed a pronounced density dependence of its oligomeric assembly, which seemed to saturate at a level of ~ 2.8 transporter molecules per oligomer (Fig. 4c). Repetitive TOCCSL runs revealed rapid protomer exchange (Fig. 4d). Together, mGFP-SERT K352A-K460A behaved similar as wild-type SERT after PIP₂ depletion.

Discussion

Although there is a wealth of data supporting the existence of neurotransmitter transporters in oligomeric quaternary structures¹⁰, the nature of the interaction between the subunits has yet not been unravelled. Here, we examined the size and stability of oligomeric complexes of SERT at two different subcellular localizations, the ER membrane and the plasma membrane. We found that dynamic equilibration of SERT oligomers occurs at the ER membrane. After trafficking through the secretory pathway, the pre-formed oligomers undergo kinetic trapping at the plasma membrane. Pre-equilibration of subunit binding at the ER membrane and kinetic trapping of oligomerized protomers at the plasma membrane enables the cell to spatially decouple the oligomerization process from the final site of oligomer operation.

This appears crucial to render the degree of oligomerization unsusceptible to different SERT concentrations at various localizations on the plasma membrane.

Our data indicate that the phosphoinositide PIP₂ plays an essential role in this process and that the different PIP₂ concentrations of the ER membrane and the plasma membrane are responsible for the pronounced differences. While other phosphoinositides would also be plausible candidates for mediating charge-induced SERT oligomerization, some lines of evidence indicate the specific role of PIP₂ in this process. First, PLC_γ is a highly specific enzyme for PIP₂ hydrolysis, leaving other phosphoinositides virtually unaffected²⁹. Experiments shown in Fig. 3 hence reveal the specific contribution of PIP₂ to SERT oligomerization. Second, PIP₂ is by far the most common phosphoinositide in the plasma membrane¹⁶, thereby outcompeting other phosphoinositide species by sheer concentration effects. Third, due to rapid dephosphorylation the ER membrane contains phosphatidylinositol (PI) and phosphatidylinositol(4)phosphate (PI(4)P), but virtually no PIP₂ or other multi-phosphorylated phosphoinositides¹⁶. Figures 1 and 2 thus render a role of PI and PI(4)P in SERT oligomerization unlikely.

In the following, we propose a model how PIP₂ may cause kinetic trapping of SERT oligomers at the plasma membrane (Fig. 5), which has three cornerstones:

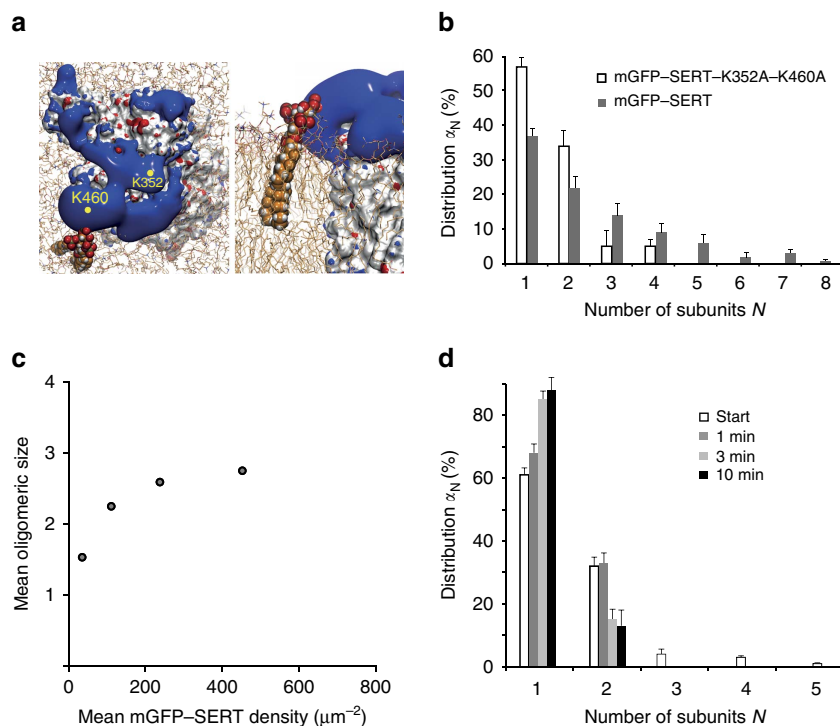


Figure 4 | Direct binding of PIP₂ to SERT mediates oligomerization. (a) Analysis of the electrostatic field generated by SERT. The final structure of a 100 ns simulation of a membrane-inserted SERT is shown as viewed from the cytosol (left) or in side-view (right). SERT surface is shown in white, the electrostatic isosurfaces in red (negative potential) and blue (positive potential). For illustration purposes, a PIP₂ molecule was placed into the membrane (in space filled representation) in close proximity to the large positively charged area that includes residue K460. (b) We determined the quaternary assembly of the mutant mGFP-SERT-K352A-K460A at the plasma membrane (white bars). Proteins were expressed at a surface density of 83 ± 31 (s.e.m.) molecules μm^{-2} . A distinctive shift to monomers and dimers compared with the wild type (grey bars) was observed ($n=23$ cells). (c) A pronounced dependence of mean oligomeric state on mGFP-SERT-K352A-K460A surface density was observed, which saturates around 2.8 transporter molecules per oligomer ($n>19$ cells per datapoint; plotted protein densities are 35 ± 11 (s.e.m.) μm^{-2} , $110 \pm 33 \mu\text{m}^{-2}$, $237 \pm 14 \mu\text{m}^{-2}$ and $452 \pm 35 \mu\text{m}^{-2}$; s.e.m. of mean oligomeric sizes were smaller than 0.05). (d) Repetitive TOCCSL runs revealed rapid protomer exchange kinetics for this mutant ($n=18$ cells). Error bars show the s.e.m.

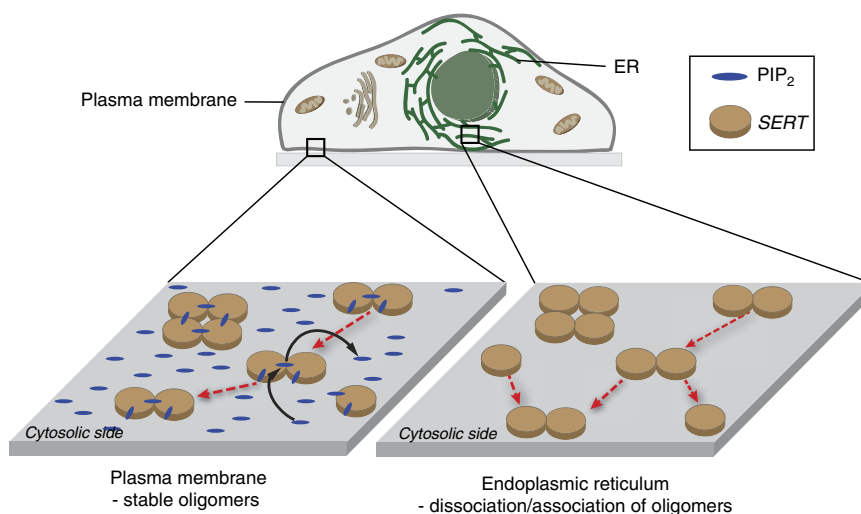


Figure 5 | A model for PIP₂ dependent oligomerization of SERT. High PIP₂ concentrations at the plasma membrane (left) saturates PIP₂ binding sites on SERT, impeding further oligomerization of the subunits. Also disassembly of the oligomers is efficiently prevented: in case of PIP₂ unbinding, the vacant position is rapidly re-populated by a new PIP₂ molecule before the protomers can separate by diffusion. Together, the two effects lead to the kinetic trapping of the oligomeric state at the plasma membrane. At the ER membrane, however, low PIP₂ concentrations lead to coexistence of PIP₂-ligated and -unligated SERT (right), which are capable of mutual binding. Hence, such conditions enable fast equilibration of the oligomerization process, including subunit exchange between SERT oligomers.

- (i) two negatively charged phosphate groups on PIP₂ bind electrostatically to positively charged patches on the cytosolic face of two SERT molecules

SERT contains a patch with a strong positive electrostatic potential on the intracellular face which is in contact with the polar headgroups of the membrane²⁰ (Fig. 4b). The cationic patch is generated by basic amino acid residues (including K352 and K460). The inositol sugar ring of PIP₂ has two functional PO₄⁻² groups in position 4 and 5, each harbouring a negative charge of -2 (ref. 30). These functional PO₄⁻² groups are oriented towards opposing ends of the inositol ring and would therefore have the possibility to interact with two separate SERT monomers. Thereby, they would effectively act as an ionic bridge between the two SERT transporters.

- (ii) abrogation of PIP₂ binding leads to rapid equilibration of the oligomerization process

The oligomerization process of SERT rapidly equilibrates under conditions, where PIP₂ does not contribute to the subunit association process. This was inferred from the results of three different approaches: the depletion of PIP₂ by enzymatic conversion to IP₃ and diacylglycerol by activation of PLC γ (Fig. 3); the retention of SERT in the ER, where PIP₂ levels are extremely low³¹ (Figs 1c and 2c); the reduction of PIP₂ binding by introduction of two point mutations²⁰ (Fig. 4). All conditions revealed qualitatively similar behaviour, that is, the mean size of SERT oligomers became dependent on SERT surface density, and protomers exchanged rapidly between different oligomers. Intrinsic low affinity protein–protein interactions between SERT protomers seem to mediate this process, however, contributions of low PIP₂ concentrations cannot be ruled out. Of note, equilibration of receptor oligomerization at the ER membrane was recently reported for a GPCR³².

At this stage, we do not know at which exact subcellular location oligomerization is ultimately adjusted; low PIP₂ levels in virtually all subcellular membranes except for the plasma membrane suggest that the exchange of subunits remains rapid until the fusion of the cargo vesicles with the plasma membrane.

- (iii) elevated PIP₂ levels saturate PIP₂ binding sites on SERT, thereby stabilizing the oligomer

In principle, PIP₂ binding to the polybasic patch at the cytosolic face of SERT, which includes the lysine residues in positions 352 and 460, increases the affinity to other, undecorated SERT protomers. Naturally occurring concentrations of PIP₂ at the plasma membrane (~20,000–60,000 molecules μm^{-2} ; (ref. 33)), however, lead to saturation of SERT with PIP₂, thereby imposing a charge-based repulsive interaction which precludes further oligomerization.

In consequence, over time most oligomers would disassemble to monomeric SERT until equilibrium is reached, where virtually only PIP₂-decorated monomers would be present. Importantly, however, there are mechanisms which strongly slow down this equilibration process ('kinetic trapping'). In fact, the high PIP₂ concentration itself may account for such a mechanism. Following this line of argumentation, SERT disassembly may require the complete dissociation of one or several PIP₂ molecules. The high PIP₂ concentrations at the plasma membrane would result in immediate replenishment of the vacant position before separation of the individual protomers.

Hence, according to our model PIP₂ levels are not responsible for tuning the oligomeric distribution of SERT, but instead determine the kinetics for reaching the equilibrium of the

oligomerization process: at low PIP₂ levels (as present at the ER membrane) equilibration is fast, whereas at high PIP₂ levels (as present at the plasma membrane) equilibration is substantially slowed down.

In summary, our data show two important steps in the oligomerization of a transmembrane protein: (i) pre-equilibration of subunit binding at the ER membrane and (ii) kinetic trapping of oligomerization at the plasma membrane. By this, the oligomerization process becomes spatially decoupled from the final site of oligomer operation. This could be important to make the degree of oligomerization insensitive to different SERT concentrations at various locations on the plasma membrane.

Methods

mGFP-SERT construct. eGFP in the pEGFP-C1 vector (Clontech) was converted to mGFP^{34,35} by mutating alanine 207 of eGFP to lysine using Quik-Change mutagenesis Kit XL from Agilent technologies (Primer: Fw: 5'-TAC CTG AGC ACC CAG TCC AAA CTG AGC AAA GAC CCC AAC-3', rev: 5'-GTT GGG GTC TTT GCT CAG TTT GGA CTG GGT GCT CAG GTA-3'). cDNAs of WT human SERT and the mutated version SERT-K352A-K460A (ref. 20) were cloned to the mutated vector via HindIII and XhoI restriction sites. For full sequence see Supplementary Note 1. Functionality of mGFP-SERT and mGFP-SERT-K352A-K460A was proven by uptake experiments as described before^{20,36}.

Cell culture. CHO cells were cultured at 37 °C and 5% CO₂ in Dulbecco's modified Eagle's medium (DMEM, PAA Laboratories) supplemented with 10% FCS (Invitrogen), penicillin and streptomycin. Cell lines are tested monthly for mycoplasma contamination using MycoAlert (Lonza).

Generation of stable cell lines. A CHO cell line (European Collection of Authenticated Cell Cultures) stably expressing mGFP-SERT was generated; transient transfection using the FuGENE 6 transfection kit (Promega) was performed according to the manufacturer's instructions. A total of 6 μg DNA per 10 cm dish was used. The cells were cultured at 37 °C and 5% CO₂ in DMEM F-12 Ham's (DMEM F-12 HAMS, PAA Laboratories) supplemented with 10% FCS (Invitrogen), penicillin and streptomycin. After 5 days, 800 $\mu\text{g ml}^{-1}$ of G418 (Sigma-Aldrich) was added as a selection marker for stably transfected cells. After 4 weeks the surviving cells were FACS sorted according to their emission in the 488 nm laser line. Only cells showing clear mGFP expression were used for further incubation. Polyclonal cultures were used to ensure a sufficient range of expression levels for density dependent experiments. The cells were further cultured in DMEM F-12 HAMS supplemented with 10% FBS, penicillin, streptomycin and 400 $\mu\text{g ml}^{-1}$ of G418.

Prevention of mGFP-SERT trafficking from the ER. To retain mGFP-SERT in the ER, a dominant-negative mutant of Sar1a (Sar1a-T39N) was used for co-transfection of CHO cells with mGFP-SERT¹³. A quantity of 990 ng of the expression vector encoding Sar1a-T39N was mixed with 10 ng of mGFP-SERT containing plasmid, ensuring that all transfected cells showed retention of mGFP-SERT in the ER. For all experiments, imaging was performed 12–20 h after the transfection, thereby ensuring similar GFP maturation times.

Coating of glass slides. Proper attachment of the cell lines was ensured by coating the glass slides with fibronectin (Invitrogen) as follows: the slides were cleaned in 70% ethanol supplemented with 2% hydrochloric acid for 15 min and washed three times for 5 min in dH₂O. 90 μl fibronectin (50 $\mu\text{g ml}^{-1}$ in 1 \times PBS) was uniformly distributed on the glass and dried at 50 °C. Unbound fibronectin was removed by washing the glass slides three times with 1 \times PBS (PAA Laboratories) before use.

PIP₂ depletion experiments were performed on glass slides coated with poly-D-lysine (PDL, Sigma Aldrich). Cleaned slides were incubated with 0.1 mg ml⁻¹ PDL for 1 h at 37 °C and washed three times before use.

Microscopy. A 488 nm laser (SAPPHIRE HP, Coherent Inc.) was mode-cleaned using a pinhole and the illumination intensity and timing were adjusted with an acousto-optical modulator (model 1205, Isomet) using a custom written software (Labview, National Instruments). The laser beam was focused onto the back-focal plane of a TIRF objective (NA 1.46, $\times 100 \times$ Plan APOCHROMAT, Zeiss) mounted on an inverted Zeiss Axiovert 200 microscope. The emission light was filtered using appropriate filter sets for GFP and imaged with a back-illuminated liquid nitrogen cooled CCD camera (Micro Max 1300-PB, Roper Scientific). To restrict the excitation and photobleaching area an adjustable slit aperture (Zeiss) was used as field stop.

All experiments were performed at room temperature. Imaging during all experiments was performed using an objective-type TIRF excitation with an excitation power of $\sim 0.5\text{--}0.8\text{ kW cm}^{-2}$ (determined in epi-configuration) and stroboscopic illumination with excitation times of 3 ms.

Fluorescence recovery after photobleaching. To determine the mobile fraction of mGFP-SERT, an $\sim 7 \times 7\ \mu\text{m}$ area of the bottom plasma membrane or the plasma membrane-proximal ER was irreversibly photobleached, and the fluorescence recovery over time was monitored ($n > 10$ cells). Photobleaching and readout were performed in TIRF configuration. Data were analysed using in-house algorithms implemented in Matlab. The central part of the bleached region was evaluated by integrating all counts and normalizing to the pre-bleach image. For calculation of the mobile fraction α of mGFP-SERT the resulting curve was fitted with $\frac{I}{I_0} = \alpha \times (1 - \exp(-\frac{t}{\tau}))$.

TOCCSL. TOCCSL experiments were performed as follows (Supplementary Fig. 2). A pre-bleach image was recorded, which was used for determination of the SERT surface density. After a $t_{\text{pre}} = 50$ ms, a confined region of the cell membrane was photobleached for $t_{\text{bleach}} = 600\text{--}800$ ms with a high laser power of $\sim 5\text{--}7\text{ kW cm}^{-2}$. To check for complete bleaching, a post-bleach image was recorded $t_{\text{post}} = 40$ ms after the bleach pulse. Finally, the TOCCSL image was recorded after an adjustable recovery time of $t_{\text{recovery}} = 1,500\text{--}12,000$ ms. Images were acquired at low excitation power of $\sim 0.5\text{--}0.8\text{ kW cm}^{-2}$ (all excitation intensities were determined in epi-configuration).

Brightness analysis. For single-molecule analysis, images were analysed using in-house algorithms implemented in MATLAB (MathWorks). Individual diffraction-limited signals were selected and fitted with a Gaussian intensity profile. The fitting routine yielded the single spot brightness B , which was used to determine the oligomeric state of SERT^{7,26,27,37}. The obtained brightness values of each diffraction-limited spot in the TOCCSL image were plotted as a pdf $\rho(B)$. To obtain the brightness distribution of single mGFP molecules $\rho_1(B)$, cells were extensively photobleached, which reduced the amount of active fluorophores to a few molecules per μm^2 , so that each potential mGFP-SERT oligomer contained only one active fluorophore at maximum. By autoconvolution, the monomer brightness distribution was used to calculate the brightness distributions for dimers $\rho_2(B)$, trimers $\rho_3(B)$ and so on. The overall single spot brightness distribution $\rho(B)$ was then fitted by a linear combination of $\rho_1(B)$, $\rho_2(B)$, $\rho_3(B)$ and so on:

$$\rho(B) = \sum_{N=1}^{N_{\text{max}}} \alpha_N \cdot \rho_N(B) \quad (1)$$

Fitting $\rho(B)$ with equation (1) yielded the fractions α_N of the different numbers of co-diffusing active mGFP molecules (with the number of mGFP molecules; Supplementary Fig. 3). Note that α_N is proportional to the oligomeric size of SERT, but—due to incomplete mGFP maturation—it slightly underestimates the degree of SERT oligomerization³⁸.

At least 750 datapoints were used for n -mer calculations. Using simulation approaches, this sample size was shown to be sufficient for obtaining statistically significant results³⁹. To determine error bars, we performed a bootstrapping analysis. Briefly, randomly chosen subsamples containing 50% of the data were analysed using equation (1); shown error bars represent the obtained s.d. from 100 repetitions for each oligomeric size divided by $\sqrt{2}$.

Mean oligomeric sizes were determined by $N_{\text{mean}} = \frac{\sum_{N=1}^{N_{\text{max}}} N \cdot \alpha_N}{\sum_{N=1}^{N_{\text{max}}} \alpha_N}$.

Repetitive TOCCSL experiments. To study oligomer stability, a repetitive TOCCSL protocol was applied. One TOCCSL run per minute was performed on the same region of each cell, following the timing protocol shown in Supplementary Fig. 2. Single runs were repeated over 10 min starting from the first bleach pulse. Both bleaching and image acquisition were done in TIRF mode. The TOCCSL image of each run was used for brightness analysis.

Determination of the SERT surface density. The mean fluorescence intensity per μm^2 of the bottom plasma membrane was calculated and divided by the mean single-molecule brightness of mGFP-SERT. To calculate SERT surface densities at plasma membrane-proximal ER, the area fraction of ER-PM junctions was determined from super-resolution images²³, and the mean intensity of ER-retained SERT was divided by the single-molecule brightness and the respective area fraction.

Enzymatic PIP₂ depletion. For activation of phospholipase C γ , cells were incubated for 20 min at 37 °C with 25 μM 2,4,6-trimethyl-N-[3-(trifluoromethyl)phenyl]benzenesulfonamide (m -3M3FBS, Sigma-Aldrich) in Hank's Balanced Salt Solution (HBSS), with calcium and magnesium (Sigma-Aldrich) supplemented with 2% FCS. m -3M3FBS remained in the imaging buffer during measurements. For the evaluation of the interaction kinetics (repetitive TOCCSL experiments) a concentration of 1 μM m -3M3FBS was used. As a negative control, the inactive ortho-analog o -3M3FBS (Tocris) was used.

Molecular modelling and simulations. The crystal structure of human SERT (PDB ID: 516X)⁴⁰ was used as starting structure. The missing side chains were modelled with MODELLER version 9.15 (ref. 41), creating 100 models using the automodel procedure. The best three models, selected according to the DOPE score⁴², were inserted into a 1-palmitoyl-2-oleoyl-sn-glycero-3-phosphatidylcholine containing membrane using the membed procedure⁴³. The membrane was pre-equilibrated to contain the SERT transporter⁴⁴. The system was electroneutralized and 150 mM NaCl were added. The environment of SERT was equilibrated while position restraining the transporter. SERT was then released by reducing the position restraints on SERT in four steps, applying 1,000, 100, 10 and 1 kJ mol⁻¹, respectively, each time simulating for 2.5 ns. Production runs of 100 ns long equilibrium molecular dynamics simulations were carried out with the GROMACS 5.1 MD package⁴⁵ using the AMBER force field⁴⁶ for the protein and the Berger parameters⁴⁷ for the membrane. The system was maintained at 310 K while coupling protein, membrane and solvent independently using the v-rescale thermostat⁴⁸. The pressure was maintained at 1 bar using the weak coupling algorithm, electrostatic interactions were calculated using the smooth particle mesh Ewald method⁴⁹ with a 1.0 nm cutoff. Lennard-Jones interactions were evaluated applying a 1.0 nm cutoff. Long range corrections for energy and pressure were applied.

Code availability. The Matlab Source code for TOCCSL analysis is available at https://github.com/schuetzgroup/TOCCSL_analysis.

Data availability. Data supporting the findings of this study are available within the article and its Supplementary Information Files and from the corresponding author upon reasonable request. The PDB accession code 516X (SERT Structure) was used in this work.

References

- Saier, M. H., Tran, C. V. & Barabote, R. D. TCDB: the transporter classification database for membrane transport protein analyses and information. *Nucleic Acids Res.* **34**, D181–D186 (2006).
- Schloss, P. & Williams, D. C. The serotonin transporter: a primary target for antidepressant drugs. *J. Psychopharmacol.* **12**, 115–121 (1998).
- Kristensen, A. S. *et al.* SLC6 neurotransmitter transporters: structure, function, and regulation. *Pharmacol. Rev.* **63**, 585–640 (2011).
- Sitte, H. H. & Freissmuth, M. Amphetamines, new psychoactive drugs and the monoamine transporter cycle. *Trends Pharmacol. Sci.* **133**, 163–166 (2015).
- Schmid, J. A. *et al.* Oligomerization of the human serotonin transporter and of the rat GABA transporter 1 visualized by fluorescence resonance energy transfer microscopy in living cells. *J. Biol. Chem.* **276**, 3805–3810 (2001).
- Just, H., Sitte, H. H., Schmid, J. A., Freissmuth, M. & Kudlacek, O. Identification of an additional interaction domain in transmembrane domains 11 and 12 that supports oligomer formation in the human serotonin transporter. *J. Biol. Chem.* **279**, 6650–6657 (2004).
- Anderlueh, A. *et al.* Single molecule analysis reveals coexistence of stable serotonin transporter monomers and oligomers in the live cell plasma membrane. *J. Biol. Chem.* **289**, 4387–4394 (2014).
- Kilic, F. & Rudnick, G. Oligomerization of serotonin transporter and its functional consequences. *Proc. Natl Acad. Sci. USA* **97**, 3106–3111 (2000).
- Jess, U., Betz, H. & Schloss, P. The membrane-bound rat serotonin transporter, SERT1, is an oligomeric protein. *FEBS Lett.* **394**, 44–46 (1996).
- Sitte, H. H., Farhan, H. & Javitch, J. A. Sodium-dependent neurotransmitter transporters: oligomerization as a determinant of transporter function and trafficking. *Mol. Interv.* **4**, 38–47 (2004).
- Scholz, P., Freissmuth, M. & Sitte, H. H. Mutations within an intramembrane leucine heptad repeat disrupt oligomer formation of the Rat GABA transporter 1. *J. Biol. Chem.* **277**, 43682–43690 (2002).
- Farhan, H., Freissmuth, M. & Sitte, H. H. in *Neurotransmitter Transporters* Vol. 175 (eds Sitte, H. & Freissmuth, M.) 233–249 (Springer, 2006).
- Farhan, H. *et al.* Concentrative export from the endoplasmic reticulum of the γ -aminobutyric acid transporter 1 requires binding to SEC24D. *J. Biol. Chem.* **282**, 7679–7689 (2007).
- Sucic, S. *et al.* Switching the clientele: a lysine residing in the C terminus of the serotonin transporter specifies its preference for the coat protein complex II component SEC24C. *J. Biol. Chem.* **288**, 5330–5341 (2013).
- Seidel, S. *et al.* Amphetamines take two to tango: an oligomer-based counter-transport model of neurotransmitter transport explores the amphetamine action. *Mol. Pharmacol.* **67**, 140–151 (2005).
- Di Paolo, G. & De Camilli, P. Phosphoinositides in cell regulation and membrane dynamics. *Nature* **443**, 651–657 (2006).
- Hilgemann, D. W. Local PIP₂ signals: when, where, and how? *Pflügers Archiv.—Eur. J. Physiol.* **455**, 55–67 (2007).

18. Tran, D. *et al.* Cellular distribution of polyphosphoinositides in rat hepatocytes. *Cell. Signal.* **5**, 565–581 (1993).
19. Suh, B.-C. & Hille, B. PIP₂ is a necessary cofactor for ion channel function: how and why? *Annu. Rev. Biophys.* **37**, 175–195 (2008).
20. Buchmayer, F. *et al.* Amphetamine actions at the serotonin transporter rely on the availability of phosphatidylinositol-4,5-bisphosphate. *Proc. Natl Acad. Sci. USA* **110**, 11642–11647 (2013).
21. Hamilton, P. J. *et al.* PIP₂ regulates psychostimulant behaviors through its interaction with a membrane protein. *Nat. Chem. Biol.* **10**, 582–589 (2014).
22. Fenollar-Ferrer, C. *et al.* Structure and regulatory interactions of the cytoplasmic terminal domains of serotonin transporter. *Biochemistry* **53**, 5444–5460 (2014).
23. Anderluh, A. *et al.* Tracking single serotonin transporter molecules at the endoplasmic reticulum and plasma membrane. *Biophys. J.* **106**, L33–L35 (2014).
24. Nagaya, H. *et al.* Regulated motion of glycoproteins revealed by direct visualization of a single cargo in the endoplasmic reticulum. *J. Cell Biol.* **180**, 129–143 (2008).
25. Moertelmaier, M., Brameshuber, M., Linimeier, M., Schütz, G. J. & Stockinger, H. Thinning out clusters while conserving stoichiometry of labeling. *Appl. Phys. Lett.* **87**, 263903 (2005).
26. Brameshuber, M. *et al.* Imaging of mobile long-lived nanoplateforms in the live cell plasma membrane. *J. Biol. Chem.* **285**, 41765–41771 (2010).
27. Madl, J. *et al.* Resting state orai1 diffuses as homotetramer in the plasma membrane of live mammalian cells. *J. Biol. Chem.* **285**, 41135–41142 (2010).
28. Bae, Y. S. *et al.* Identification of a compound that directly stimulates phospholipase C activity. *Mol. Pharmacol.* **63**, 1043–1050 (2003).
29. Kadamur, G. & Ross, E. M. Mammalian phospholipase C. *Annu. Rev. Physiol.* **75**, 127–154 (2013).
30. Kooijman, E. E., King, K. E., Gangoda, M. & Gericke, A. Ionization properties of phosphatidylinositol polyphosphates in mixed model membranes. *Biochemistry* **48**, 9360–9371 (2009).
31. Stefan, C. J. *et al.* Osh proteins regulate phosphoinositide metabolism at ER-plasma membrane contact sites. *Cell* **144**, 389–401 (2011).
32. Teichmann, A. *et al.* The Specific monomer/dimer equilibrium of the corticotropin-releasing factor receptor type 1 is established in the endoplasmic reticulum. *J. Biol. Chem.* **289**, 24250–24262 (2014).
33. Hilgemann, D. Local PIP₂ signals: when, where, and how? *Pflügers Archiv.—Eur. J. Physiol.* **455**, 55–67 (2007).
34. Zacharias, D. A., Violin, J. D., Newton, A. C. & Tsien, R. Y. Partitioning of lipid-modified monomeric GFPs into membrane microdomains of live cells. *Science* **296**, 913–916 (2002).
35. Yang, A. *et al.* A chemical biology route to site-specific authentic protein modifications. *Science* **354**, 623–626 (2016).
36. Susic, S. *et al.* The N terminus of monoamine transporters is a lever required for the action of amphetamines. *J. Biol. Chem.* **285**, 10924–10938 (2010).
37. Schmidt, T., Schütz, G. J., Gruber, H. J. & Schindler, H. Local stoichiometries determined by counting individual molecules. *Anal. Chem.* **68**, 4397–4401 (1996).
38. Ulbrich, M. H. & Isacoff, E. Y. Subunit counting in membrane-bound proteins. *Nat. Methods* **4**, 319–321 (2007).
39. Brameshuber, M. & Schutz, G. J. Detection and quantification of biomolecular association in living cells using single-molecule microscopy. *Methods Enzymol.* **505**, 159–186 (2012).
40. Coleman, J. A., Green, E. M. & Gouaux, E. X-ray structures and mechanism of the human serotonin transporter. *Nature* **532**, 334–339 (2016).
41. Šali, A. & Blundell, T. L. Comparative protein modelling by satisfaction of spatial restraints. *J. Mol. Biol.* **234**, 779–815 (1993).
42. Shen, M.-Y. & Sali, A. Statistical potential for assessment and prediction of protein structures. *Protein Sci.* **15**, 2507–2524 (2006).
43. Wolf, M. G., Hoefling, M., Aponte-Santamaria, C., Grubmüller, H. & Groenhof, G. g_membed: Efficient insertion of a membrane protein into an equilibrated lipid bilayer with minimal perturbation. *J. Comput. Chem.* **31**, 2169–2174 (2010).
44. Koban, F. *et al.* A salt bridge linking the first intracellular loop with the C terminus facilitates the folding of the serotonin transporter. *J. Biol. Chem.* **290**, 13263–13278 (2015).
45. Hess, B., Kutzner, C., van der Spoel, D. & Lindahl, E. GROMACS 4: algorithms for highly efficient, load-balanced, and scalable molecular simulation. *J. Chem. Theory Comput.* **4**, 435–447 (2008).
46. Lindorff-Larsen, K. *et al.* Improved side-chain torsion potentials for the Amber ff99SB protein force field. *Proteins* **78**, 1950–1958 (2010).
47. Berger, O., Edholm, O. & Jähnig, F. Molecular dynamics simulations of a fluid bilayer of dipalmitoylphosphatidylcholine at full hydration, constant pressure, and constant temperature. *Biophys. J.* **72**, 2002–2013 (1997).
48. Bussi, G., Donadio, D. & Parrinello, M. Canonical sampling through velocity rescaling. *J. Chem. Phys.* **126**, 014101 (2007).
49. Darden, T., York, D. & Pedersen, L. Particle mesh Ewald: an Nlog(N) method for Ewald sums in large systems. *J. Chem. Phys.* **98**, 10089–10092 (1993).

Acknowledgements

This work was supported by the Austrian Science Fund/FWF (F3506-B20 and W1232 to H.H.S., F3519-B20 to G.J.S. and F3524-B20 to T.S.). E.K. acknowledges funding from in part FEBS Long-term Fellowship and the ARC DECRA Fellowship.

Author contributions

A.A. performed the measurements and data analysis. T.H. and O.K. provided expression vectors and stably expressing cell lines. A.A., T.H., E.K., T.S., H.H.S. and G.J.S. designed the experiments. T.S. performed computational modelling. A.A., G.J.S., H.H.S. and T.S. wrote the manuscript. All authors participated in the discussion of results and contributed to the preparation of the manuscript.

Additional information

Supplementary Information accompanies this paper at <http://www.nature.com/naturecommunications>

Competing financial interests: The authors declare no competing financial interests.

Reprints and permission information is available online at <http://npg.nature.com/reprintsandpermissions/>

How to cite this article: Anderluh, A. *et al.* Direct PIP₂ binding mediates stable oligomer formation of the serotonin transporter. *Nat. Commun.* **8**, 14089 doi: 10.1038/ncomms14089 (2017).

Publisher's note: Springer Nature remains neutral with regard to jurisdictional claims in published maps and institutional affiliations.



This work is licensed under a Creative Commons Attribution 4.0 International License. The images or other third party material in this article are included in the article's Creative Commons license, unless indicated otherwise in the credit line; if the material is not included under the Creative Commons license, users will need to obtain permission from the license holder to reproduce the material. To view a copy of this license, visit <http://creativecommons.org/licenses/by/4.0/>

© The Author(s) 2017